DECAYING TURBULENCE AS A FRACTAL CURVE

Alexander Migdal [1,†,‡] ⬤

[1]   Department of Physics, New York University Abu Dhabi, Saadiyat Island, Abu Dhabi, PO Box 129188, Abu Dhabi, United Arab Emirates; am10485@nyu.edu

Abstract: We have found an infinite dimensional manifold of exact solutions of the Navier-Stokes loop equation for the Wilson loop in decaying Turbulence in arbitrary dimension $d > 2$. This solution family is equivalent to a fractal curve in complex space $\mathbb{C}^d$ with random steps parametrized by Ising variables $\sigma = \pm 1$. This equivalence provides a **dual** theory describing a strong turbulent phase of the Navier-Stokes flow in $\mathbb{R}_d$ space as a random geometry in a different space, like ADS/CFT correspondence in gauge theory. This one-dimensional periodic Ising chain has some long-range interaction, leading to critical phenomena as its size $N \to \infty$. The Wilson loop, vorticity correlation functions, and energy dissipation rate are numerically simulated using an ensemble of $2 * 10^5$ curves, each with $N = 2 * 10^8$ steps. We found anomalous dissipation and some scaling laws with universal critical indexes, different from K41.

0. Introduction

A while ago, we derived [1,2] a functional equation for the so-called loop average [3,4] or Wilson loop in Turbulence. The path to an exact solution by a dimensional reduction in this equation was proposed in the '93 paper [2] but has just been explored.

At the time, we could not compare a theory with anything but crude measurements in physical and numerical experiments at modest Reynolds numbers. All these experiments agreed with the K41 scaling, so the exotic equation based on unjustified methods of quantum field theory was premature.

The specific prediction of the Loop equation, namely the Area law [2], could not be verified in DNS at the time with existing computer power.

The situation has changed over the last decades. No alternative microscopic theory based on the Navier-Stokes equation emerged, but our understanding of the strong turbulence phenomena grew significantly.

On the other hand, the loop equations technology in the gauge theory also advanced over the last decades. The correspondence between the loop space functionals and the original vector fields was better understood, and various solutions to the gauge loop equations were found.

In particular, the momentum loop equation was developed, similar to our momentum loop used below [5–7]. Recently, some numerical methods were found to solve loop equations beyond perturbation theory [8,9].

The loop dynamics was extended to quantum gravity, where it was used to study nonperturbative phenomena [10,11].

All these old and new developments made loop equations a major nonperturbative approach to gauge field theory.

So, it is time to revive the hibernating theory of the loop equations in Turbulence, where these equations are much simpler.

The latest DNS [12–15] with Reynolds numbers of tens of thousands revealed and quantified violations of the K41 scaling laws. These numerical experiments are in agreement with so-called multifractal scaling laws [16].

However, as we argued in [17,18], at those Reynolds numbers, the DNS cannot yet distinguish between pure scaling laws with anomalous dimension $\zeta(n)$ and some algebraic function of the logarithm of scale $\zeta(n, \log r)$ modifying the K41 scaling.

Theoretically, we studied the loop equation in the confinement region (large circulation over large loop C), and we have justified the Area law, suggested back in '93 on heuristic arguments [2].

This law says that the tails of velocity circulation PDF in the confinement region are functions of the minimal area inside this loop.

It was verified in DNS four years ago [12] which triggered the further development of the geometric theory of turbulence[13–15,17–30].

In particular, the Area law was justified for flat and quadratic minimal surfaces [22], and an exact scaling law in confinement region $\Gamma \propto \sqrt{Area}$ was derived [21]. The area law was verified with better precision in [13].

It was later conjectured in [17] that the dominant field configurations in extreme Turbulence are so-called Kelvinons, which were shown to solve stationary Navier-Stokes equations assuming the sparse distribution of vorticity structures.

These topological solitons of the Euler theory are built around a vortex sheet bounded by a singular vortex line. This vortex line is locally equivalent to the cylindrical Burgers vortex [31], with infinitesimal thickness in the limit of a large Reynolds number.

As we argued in [17,18], the Kelvinon has an anomalous dissipation, surviving the strong turbulent limit. This dissipation is proportional to the square of constant circulation of the Burgers vortex times a line integral of the tangent component of the strain along the loop.

The Kelvinon minimizes the energy functional, with anomalous terms coming from the Burgers core of the vortex line. There is also a constant scale factor Z in the representation of the Kelvinon vorticity in terms of spherical Clebsch variables:

$$\vec{\omega} = 1/2 Z e_{abc} S_a \vec{\nabla} S_b \times \vec{\nabla} S_c = \vec{\nabla} \phi_1 \times \vec{\nabla} \phi_2; \tag{1}$$

$$S_1^2 + S_2^2 + S_3^2 = 1; \tag{2}$$

$$\phi_2 = \arg\left(S_1 + \imath S_2\right); \; \phi_1 = Z S_3; \tag{3}$$

In that paper, the constant Z was related to the Kolmogorov energy dissipation density and the boundary value of the S_3 variable at the loop C.

The anomalous Hamiltonian [17,18] explicitly violated the K41 scaling by the logarithmic terms $\log Z/\nu$ in the region of small loops C. This region resembles the asymptotically free QCD. The logarithmic terms were summed up by RG equation with running coupling constant logarithmically small in this region.

These exciting developments explain and quantitatively describe many interesting phenomena [18] but do not provide a complete microscopic theory covering the full inertial range of Turbulence without simplifying assumptions of the sparsity of vortex structures.

Moreover, while the Kelvinon (presumably) solves the stationary Navier-Stokes equations, it **does not** solve the loop equations for the following reason.

The loop equation assumes that the velocity field is **independent** of the loop C. In this case, the circulation $\oint_C v_\alpha dr_\alpha$ variations in the loop functional by the shape C of the loop can be reduced to the Navier-Stokes equation.

Otherwise, the variation would also involve the variation of the velocity field $\oint_C \delta v_\alpha dr_\alpha$.

This problem does not invalidate the Kelvinon theory as an ideal gas of random vortex rings sparsely distributed in a turbulent flow.

The loop functional is not needed for that statistical theory, and the stationary solution of the Navier-Stokes equation is sufficient. The shape of the loop and the vortex sheet inside would become random variables influenced by a background strain like in the pure vortex sheet solutions [18].

These objections, however, prevent the Kelvinon gas model from being a complete theory of strong isotropic Turbulence. This model is merely an approximation of the full theory.

In the present work, we develop the theory free of these assumptions and approximations by exactly solving the loop equations for decaying Turbulence.

1. Loop equation

1.1. Loop operators

We introduced the loop equation in Lecture Series at Cargese and Chernogolovka Summer Schools [2].

Here is a summary for the new generation.

We write the Navier-Stokes equation as follows

$$\partial_t v_\alpha = \nu \partial_\beta \omega_{\beta\alpha} - v_\beta \omega_{\beta\alpha} - \partial_\alpha \left(p + \frac{v_\beta^2}{2} \right); \tag{4}$$

$$\partial_\alpha v_\alpha = 0; \tag{5}$$

The Wilson loop average for the Turbulence

$$\Psi[\gamma, C] = \left\langle \exp\left(\frac{\imath \gamma}{\nu} \oint_C v_\alpha dr_\alpha \right) \right\rangle \tag{6}$$

treated as a function of time and a functional of the periodic function $C : r_\alpha = C_\alpha(\theta); \ \theta \in (0, 2\pi)$ (not necessarily a single closed loop), satisfies the following functional equation

$$\imath \nu \partial_t \Psi = \mathcal{H}_C \Psi; \tag{7a}$$

$$\mathcal{H}_C = \mathcal{H}_C^{(1)} + \mathcal{H}_C^{(2)} \tag{7b}$$

$$\mathcal{H}_C^{(1)} = \nu\gamma \oint_C dr_\alpha \partial_\beta \hat{\omega}_{\alpha\beta}(r); \tag{7c}$$

$$\mathcal{H}_C^{(2)} = \gamma \oint_C dr_\alpha \hat{\omega}_{\alpha\beta}(r) \hat{v}_\beta(r); \tag{7d}$$

$$\hat{\omega}_{\alpha\beta} \equiv -\imath \frac{\nu}{\gamma} \frac{\delta}{\delta \sigma_{\alpha\beta}} \tag{7e}$$

$$\hat{v}_\beta(r) = \frac{1}{\partial_\mu^2} \partial_\alpha \hat{\omega}_{\beta\alpha}(r) \tag{7f}$$

We added a dimensionless factor γ in the exponential compared to some previous definitions as an extra parameter of the Wilson loop. Without loss of generality, we shall assume that $\gamma > 0$. The negative γ corresponds to a complex conjugation of the Wilson loop.

In Abelian gauge theory, this parameter would be the continuous electric charge.

The statistical averaging $\langle \dots \rangle$ corresponds to initial randomized data, to be specified later.

The area derivative $\frac{\delta}{\delta \sigma_{\alpha\beta}}$ is related to the variation of the functional when the little closed loop δC is added

$$\Sigma_{\alpha\beta}(\delta C) \frac{\delta F[C]}{\delta \sigma_{\alpha\beta}(r)} = F[C + \delta C] - F[C]; \tag{8}$$

$$\Sigma_{\alpha\beta}(\delta C) = \frac{1}{2} \oint_{\delta C} r_\alpha dr_\beta \tag{9}$$

In the review, [2,18], we present the explicit limiting procedure needed to define these functional derivatives in terms of finite variations of the loop while keeping it closed.

All the operators $\partial_\mu, \hat{\omega}_{\alpha\beta}, \hat{v}_\alpha$ are expressed in terms of the spike operator

$$D_\alpha(\theta, \epsilon) = \int_{-\epsilon}^{+\epsilon} d\xi \left(1 - \frac{|\xi|}{\epsilon} \right) \frac{\delta}{\delta C_\alpha(\theta + \xi)} \tag{10}$$

The area derivative operator can be regularized as

$$\Omega_{\alpha\beta}(\theta, \epsilon) = -\imath \frac{\nu}{\gamma} \frac{\delta}{\delta C'_\alpha(\theta)} \int_{-\epsilon}^{\epsilon} d\xi \frac{\delta}{\delta C_\beta(\theta + \xi)} - \{\alpha \leftrightarrow \beta\}; \tag{11}$$

and velocity operator (with $\delta, \epsilon \to 0^+$)

$$V_\alpha(\theta, \epsilon, \delta) = \frac{1}{D_\mu^2(\theta, \epsilon)} D_\beta(\theta, \epsilon) \Omega_{\beta\alpha}(\theta, \delta); \tag{12}$$

In addition to the loop equation, every valid loop functional $F[C]$ must satisfy the Bianchi constraint [3,4]

$$\partial_\alpha \frac{\delta F[C]}{\delta \sigma_{\beta\gamma}(r)} + \mathbf{cyclic} = 0 \tag{13}$$

In three dimensions, it follows from identity $\vec{\nabla} \cdot \vec{\omega} = 0$; in general dimension $d > 3$, the dual vorticity $\tilde{\omega}$ is an antisymmetric tensor with $d - 2$ components. The divergence of this tensor equals zero identically.

However, for the loop functional, this restriction is not an identity; it reflects that this functional is a function of a circulation of some vector field, averaged by some set of parameters.

This constraint was analyzed in [18] in the confinement region of large loops, where it was used to predict the Area law. The area derivative of the area of some smooth surface inside a large loop reduces to a local normal vector. The Bianchi constraint is equivalent to the Plateau equation for a minimal surface (mean external curvature equals zero).

In the Navier-Stokes equation, we did NOT add artificial random forces, choosing instead to randomize the initial data for the velocity field.

These ad hoc random forces would lead to the potential term [18] in the loop Hamiltonian $\mathcal{H}_C$, breaking certain symmetries needed for the dimensional reduction we study below.

With random initial data instead of time-dependent delta-correlated random forcing, we no longer describe the steady state (i.e., statistical equilibrium) but decaying Turbulence, which is also an interesting process, manifesting the same critical phenomena.

The energy is pumped in at the initial moment $t = 0$ and slowly dissipates over time, provided the viscosity is small enough, corresponding to the large Reynolds number we are studying.

1.2. Dimensional reduction

The crucial observation in [2] was that the right side of the Loop equation, without random forcing, dramatically simplifies in functional Fourier space. The dynamics of the loop field can be reproduced in an Ansatz

$$\Psi[\gamma, C] = \left\langle \exp\left(\frac{\imath \gamma}{\nu} \oint dC_\alpha(\theta) P_\alpha(\theta) \right) \right\rangle \tag{14}$$

The difference with the original definition of $\Psi[\gamma, C]$ is that our new function $P_\alpha(\theta)$ depends directly on θ rather then through the function $v_\alpha(r)$ taken at $r_\alpha = C_\alpha(\theta)$.

This transformation is the dimensional reduction $d \Rightarrow 1$ we mentioned above.

From the point of view of the quantum analogy, this Anzatz is a plane wave in the Loop space, solving the Schrödinger equation in the absence of forces (potential terms in the Hamiltonian, depending on our position C in the loop space).

The reduced dynamics must be equivalent to the Navier-Stokes dynamics of the original field. With the loop calculus developed above, we have all the necessary tools to provide this equivalence.

Let us stress an important point: the function $\vec{P}(\theta, t)$ is **independent** of the loop C. As we shall see later, it is a random variable with a universal distribution in functional space.

This independence removes our objection (see the Introduction) to the Kelvinon theory and any other Navier-Stokes stationary solutions with a singularity at fixed loop C in space.

The functional derivative, acting on the exponential in (14) could be replaced by the derivative P' as follows

$$\frac{\delta}{\delta C_\alpha(\theta)} \leftrightarrow -\frac{\imath\gamma}{\nu} P'_\alpha(\theta) \tag{15}$$

The equation for $P(\theta)$ as a function of θ and also a function of time, reads:

$$\partial_t P_\alpha = \left(\nu D_\beta - V_\beta\right)\Omega_{\beta\alpha} \tag{16}$$

where the operators V, D, Ω should be regarded as ordinary numbers, with the following definitions.

The spike derivative D in the above equation

$$D_\alpha(\theta, \epsilon) = -\frac{\imath\gamma}{\nu} \int_{-1}^{1} d\mu \, \mathrm{sgn}(\mu) P_\alpha(\theta + \epsilon\mu) \tag{17}$$

The vorticity (11) and velocity (12) also become singular functionals of the trajectory $P(\theta)$.

The first observation about this equation is that the viscosity factor cancels after the substitution (17).

As we shall see, the viscosity enters initial data so that at any finite time t, the solution for P still depends on viscosity.

Another observation is that the spike derivative $D(\theta, \epsilon)$ turns to the discontinuity $\Delta P(\theta) = P(\theta^+) - P(\theta^-)$ in the limit $\epsilon \to 0^+$

$$D(\theta, 0^+) = -\frac{\imath\gamma}{\nu} \Delta P(\theta) \tag{18}$$

The relation of the operators in the QCD loop equation to the discontinuities of the momentum loop was noticed, justified, and investigated in [6,7].

The momentum loop could have an arbitrary number of such discontinuities and stay constant in between.

In the Navier-Stokes theory, this relation provides the key to the exact solution.

In the same way, we find the limit for vorticity

$$\Omega_{\alpha\beta}(\theta, 0^+) = \frac{-\imath\gamma}{\nu} P_{\alpha\beta}(\theta); \tag{19}$$

$$P_{\alpha\beta}(\theta) = \Delta P_\alpha(\theta) P_\beta(\theta) - \{\alpha \leftrightarrow \beta\}; \tag{20}$$

$$P_\alpha(\theta) \equiv \frac{P_\alpha(\theta^+) + P_\alpha(\theta^-)}{2} \tag{21}$$

and velocity (skipping the common argument θ)

$$V_\alpha = \frac{\Delta P_\beta}{\Delta P_\mu^2} P_{\beta\alpha} = P_\alpha - \frac{\Delta P_\alpha \Delta P_\beta P_\beta}{\Delta P^2} \tag{22}$$

The Bianchi constraint is identically satisfied as it should

$$\Delta P_\alpha \left(\Delta P_\beta P_\gamma - \{\beta \leftrightarrow \gamma\}\right) + \mathbf{cyclic} = 0 \tag{23}$$

We arrive at a singular loop equation for $P_\alpha(\theta)$

$$\frac{\nu}{\gamma}\partial_t \vec{P} = -\gamma^2(\Delta\vec{P})^2\vec{P} +$$
$$\Delta\vec{P}\left(\gamma^2\vec{P}\cdot\Delta\vec{P} + \imath\gamma\left(\frac{(\vec{P}\cdot\Delta\vec{P})^2}{\Delta\vec{P}^2} - \vec{P}^2\right)\right);\tag{24}$$

This equation is complex due to the irreversible dissipation effects in the Navier-Stokes equation.

The viscosity dropped from the right side of this equation; it can be absorbed in units of time. Viscosity also enters the initial data, as we shall see in the next Section on the example of the random rotation.

However, the large-time asymptotic behavior of the solution would be universal, as it should be in the Turbulent flow.

We are looking for a degenerate fixed point [18], a fixed manifold with some internal degrees of freedom. The spontaneous stochastization corresponds to random values of these hidden internal parameters.

Starting with different initial data, the trajectory $\vec{P}(\theta, t)$ would approach this fixed manifold at some arbitrary point and then keep moving around it, covering it with some probability measure.

The Turbulence problem is to find this manifold and determine this probability measure.

1.3. Random global vorticity

Possible initial data for the reduced dynamics were suggested in the original papers [2,18]. The initial velocity field's simplest meaningful distribution is the Gaussian one, with energy concentrated in the macroscopic motions. The corresponding loop field reads (we set $\gamma = 1$ for simplicity in this section)

$$\Psi_0[C] = \exp\left(-\frac{1}{2\nu^2}\int_C d\vec{C}(\theta)\cdot d\vec{C}(\theta')f\left(\vec{C}(\theta) - \vec{C}(\theta')\right)\right)\tag{25}$$

where $f(\vec{r})$ is the velocity correlation function

$$\langle v_\alpha(r)v_\beta(r')\rangle = \left(\delta_{\alpha\beta} - \partial_\alpha\partial_\beta\partial_\mu^{-2}\right)f(r - r')\tag{26}$$

The potential part drops out in the closed loop integral.

The correlation function varies at the macroscopic scale, which means that we could expand it in the Taylor series

$$f(r - r') \to f_0 - f_1(r - r')^2 + \dots\tag{27}$$

The first term f_0 is proportional to initial energy density,

$$\frac{1}{2}\left\langle v_\alpha^2\right\rangle = \frac{d-1}{2}f_0\tag{28}$$

and the second one is proportional to initial energy dissipation rate $\mathcal{E}_0$

$$f_1 = \frac{\mathcal{E}_0}{2d(d-1)\nu}\tag{29}$$

where $d = 3$ is the dimension of space.

The constant term in (27) as well as $r^2 + r'^2$ terms drop from the closed loop integral, so we are left with the cross-term rr', which reduces to a full square

$$\Psi_0[C] \to \exp\left(-\frac{f_1}{\nu^2}\left(\oint dC_\alpha(\theta)C_\beta(\theta)\right)^2\right) \tag{30}$$

This distribution is almost Gaussian: it reduces to Gaussian one by extra integration

$$\Psi_0[C] \to \ const \ \int (d\phi) \exp\left(-\phi_{\alpha\beta}^2\right)$$
$$\exp\left(2\imath\frac{\sqrt{f_1}}{\nu}\phi_{\mu\nu}\oint dC_\mu(\theta)C_\nu(\theta)\right) \tag{31}$$

The integration here involves all $\frac{d(d-1)}{2} = 3$ independent $\alpha < \beta$ components of the antisymmetric tensor $\phi_{\alpha\beta}$. Note that this is ordinary integration, not the functional one.

The physical meaning of this ϕ is the random uniform vorticity $\hat{\omega} = \sqrt{f_1}\hat{\phi}$ at the initial moment.

However, as we see it now, this initial data represents a spurious fixed point unrelated to the turbulence problem.

It was discussed in our review paper [18]. The uniform global rotation represents a fixed point of the Navier-Stokes equation for arbitrary uniform vorticity tensor.

Gaussian integration by ϕ keeps it as a fixed point of the Loop equation.

The right side of the Navier-Stokes equation vanishes at this special initial data so that the exact solution of the loop equation with this initial data equals its initial value (30).

Naturally, the time derivative of the momentum loop with the corresponding initial data will vanish as well.

It is instructive to look at the momentum trajectory $P_\alpha(\theta)$ for this fixed point.

The functional Fourier transform [2,18] leads to the following simple result for the initial values of $P_\alpha(\theta)$.

In terms of Fourier harmonics, this initial data read

$$P_\alpha(\theta) = \sum_{n=1}^{\infty} P_{\alpha,n}\exp(\imath n\theta) + \bar{P}_{\alpha,n}\exp(-\imath n\theta); \tag{32}$$

$$P_{\alpha,n} = \mathcal{N}(0,1)\forall\alpha, n > 0; \tag{33}$$

$$\bar{P}_{\alpha,n} = \frac{4\sqrt{f_1}}{n\nu}\phi_{\alpha\beta}P_{\beta,n};\forall\beta, n > 0; \tag{34}$$

$$\phi_{\alpha\beta} = -\phi_{\beta\alpha}; \tag{35}$$

$$\phi_{\alpha\beta} = \mathcal{N}(0,1)\forall\alpha < \beta; \tag{36}$$

As for the constant part $P_{\alpha,0}$ of $P_\alpha(\theta)$, it is not defined, but it drops from equations by translational invariance.

Note that this initial data is not real, as $\bar{P}_{\alpha,n} \neq P_{\alpha,n}^\star$. Positive and negative harmonics are real but unequal, leading to a complex Fourier transform. At fixed tensor ϕ the correlations are

$$\langle P_{\alpha,n}P_{\beta,m}\rangle_{t=0} = \frac{4\sqrt{f_1}}{m\nu}\delta_{-nm}\phi_{\alpha\beta}; \tag{37}$$

$$\langle P_\alpha(\theta)P_\beta(\theta')\rangle_{t=0} = 2\imath\frac{\sqrt{f_1}}{\nu}\phi_{\alpha\beta}\,\mathrm{sign}(\theta' - \theta); \tag{38}$$

This correlation function immediately leads to the uniform expectation value of the vorticity

$$\langle P_\alpha(\theta)\Delta P_\beta(\theta)\rangle = 4\imath\sqrt{f_1}\phi_{\alpha\beta};\ \forall\theta \tag{39}$$

The uniform constant vorticity kills the linear term of the Navier-Stokes equation in the original loop space, involving $\partial_\alpha \hat{\Omega}_{\alpha\beta} = 0$.

The nonlinear term $\hat{V}_\alpha \hat{\Omega}_{\alpha\beta}$ vanishes in the coordinate loop space only after integration around the loop.

Here are the steps involved

$$\hat{V}_\beta = \frac{1}{2}\hat{\Omega}_{\alpha\beta}C_\beta; \tag{40}$$

$$\oint \hat{\Omega}_{\alpha\beta}C_\beta\hat{\Omega}_{\beta\gamma}dC_\alpha \propto \hat{\Omega}_{\alpha\beta}\hat{\Omega}_{\beta\gamma}\Sigma_{\alpha\beta}(C); \tag{41}$$

Here the tensor area Σ was defined in (9). It is an antisymmetric tensor; therefore its trace with a symmetric tensor $\hat{\Omega}_{\alpha\beta}\hat{\Omega}_{\beta\gamma}$ vanishes.

This calculation demonstrates how an arbitrary uniform vorticity tensor satisfies the loop equation in coordinate loop space.

We expect the turbulent solution of the loop equation to be more general, with the local vorticity tensor at the loop becoming a random variable with some distribution for every point on the loop.

1.4. Decay or fixed point

The absolute value of loop average $\Psi[\gamma, C]$ stays below 1 at any time, which leaves two possible scenarios for its behavior at a large time.

$$\textbf{Decay:} \qquad \vec{P} \to 0; \ \Psi[\gamma, C] \to 1; \tag{42}$$
$$\textbf{Fixed Point:} \qquad \vec{P} \to \vec{P}_\infty; \ \Psi[\gamma, C] \to \Psi_\infty[C]; \tag{43}$$

The **Decay** scenario in the nonlinear ODE (24) corresponds to the $1/\sqrt{t}$ decrease of $\vec{P}$.

Omitting the common argument θ, we get the following **exact** time-dependent solution (not just asymptotically, at $t \to +\infty$).

$$\vec{P} = \sqrt{\frac{\nu}{2(t+t_0)}}\frac{\vec{F}}{\gamma}; \tag{44}$$

$$\left((\Delta\vec{F})^2 - 1\right)\vec{F} =$$
$$\Delta\vec{F}\left(\vec{F}\cdot\Delta\vec{F} + \frac{\imath}{\gamma}\left(\frac{(\vec{F}\cdot\Delta\vec{F})^2}{(\Delta\vec{F})^2} - \vec{F}^2\right)\right); \tag{45}$$

The **Fixed Point** would correspond to the vanishing right side of the momentum loop equation (24). Multiplying by $(\Delta\vec{P})^2$ and reducing the terms, we find a singular algebraic equation

$$\gamma^2(\Delta\vec{P})^2\left((\Delta\vec{P})^2\vec{P} - (\vec{P}\cdot\Delta\vec{P})\Delta\vec{P}\right) =$$
$$\imath\gamma\Delta\vec{P}\cdot\left((\vec{P}\cdot\Delta\vec{P})^2 - \vec{P}^2(\Delta\vec{P})^2\right); \tag{46}$$

The fixed point could mean self-sustained Turbulence, which would be too good to be true, violating the second law of Thermodynamics. Indeed, it is easy to see that this fixed point cannot exist.

The fixed point equation (46) is a linear relation between two vectors $\vec{P}, \Delta\vec{P}$ with coefficients depending on various scalar products. The generic solution is simply

$$\Delta\vec{P} = \lambda\vec{P}; \tag{47}$$

with the complex parameter λ to be determined from the equation (46).

This solution is degenerate: the fixed point equation is satisfied for arbitrary complex λ.

The discontinuity vector $\Delta \vec{P}$ aligned with the principal value $\vec{P}$ corresponds to vanishing vorticity in (19), leading to a trivial solution of the loop equation $\Psi[\gamma, C] = 1$.

We are left with the decaying turbulence scenario (45) as the only remaining physical solution.

2. Fractal curve in complex space

2.1. Random walk

One may try the solution where the discontinuity vector is proportional to the principal value. However, in this case, such a solution does not exist.

$$\Delta \vec{F} \overset{?}{=} \lambda \vec{F}; \tag{48}$$

$$\lambda^2 \vec{F}^2 - 1 \overset{?}{=} \lambda^2 \vec{F}^2; \tag{49}$$

There is, however, another solution where the vectors $\Delta \vec{F}, \vec{F}$ are not aligned. This solution requires the following relations

$$(\Delta \vec{F})^2 = 1; \tag{50a}$$

$$(2 \vec{F} \cdot \Delta \vec{F} - \imath \gamma)^2 + \gamma^2 = 4 \vec{F}^2 \tag{50b}$$

These relations are very interesting. The complex numbers reflect irreversibility, and lack of alignment leads to vorticity distributed along the loop.

Naturally, $\Delta \vec{F} = 0$ is also a solution of the loop equation (46), as this equation is local in θ. A piecewise constant curve with an arbitrary number of gaps $\Delta \vec{F}_k$ solves the loop equation, provided the gaps satisfy (50).

Also, note that this complex vector $\vec{F}(\theta)$ is dimensionless, and the fixed point equation (50) is completely universal, up to a single dimensionless parameter γ.

One can build this solution as a **Markov process** by the following method. Start with a complex vector $\vec{F}(\theta = 0) = \vec{F}_0$.

We compute the next values $\vec{F}_k = \vec{F}\left(\frac{2\pi k}{N}\right)$ from the discontinuity equations (50).

$$\left(\vec{F}_{k+1} - \vec{F}_k\right)^2 = 1; \tag{51a}$$

$$\left(\vec{F}_{k+1}^2 - \vec{F}_k^2 - \imath \gamma\right)^2 + \gamma^2 = \left(\vec{F}_{k+1} + \vec{F}_k\right)^2 \tag{51b}$$

2.2. Constraints imposed on a random step

A solution to these equations can be represented using a complex vector $\vec{q}_k$ subject to two complex constraints

$$\vec{q}_k^2 = 1; \tag{52a}$$

$$\left(2 \vec{F}_k \cdot \vec{q}_k - \imath \gamma\right)^2 = 4 \vec{F}_k^2 + \gamma(2\imath - \gamma) \tag{52b}$$

after which we can find the next value

$$\vec{F}_{k+1} = \vec{F}_k + \vec{q}_k; \tag{53}$$

We assume N steps, each with the angle shift $\Delta \theta = \frac{2\pi}{N}$.

This recurrent sequence is a Markov process because each step only depends on the current position $\vec{F}_k$. On top of this Markov process, there is a closure requirement $\vec{F}_N = \vec{F}_0$.

This requirement represents a nonlinear restriction on all the variables $\vec{F}_k$, which we discuss below.

With this discretization, the circulation can be expressed in terms of these steps

$$\oint \vec{F}(\theta) \cdot d\vec{C}(\theta) = -\oint \vec{C}(\theta) \cdot d\vec{F}(\theta) \Rightarrow -\sum_{k=0}^{N-1} \frac{\vec{C}_{k+1} + \vec{C}_k}{2} \cdot \vec{q}_k \tag{54}$$

Note that the complex unit vector is **not** defined with the Euclidean metric in six dimensions $\left\langle \vec{A}, \vec{B} \right\rangle = \mathbf{Re}\, \vec{A} \cdot \mathbf{Re}\, \vec{B} + \mathbf{Im}\, \vec{A} \cdot \mathbf{Im}\, \vec{B}$. Instead, we have a complex condition

$$\vec{q}^2 = 1 \tag{55}$$

which leads to **two** conditions between real and imaginary parts

$$(\mathbf{Re}\, \vec{q})^2 = 1 + (\mathbf{Im}\, \vec{q})^2; \tag{56}$$
$$\mathbf{Re}\, \vec{q} \cdot \mathbf{Im}\, \vec{q} = 0; \tag{57}$$

In d dimensions, there are $d - 1$ complex parameters of the unit vector; with an extra linear constraint in (52a), there are now $d - 2$ free complex parameters at every step of our iteration, plus the discrete choice of the sign of the root in the solution of the quadratic equation.

2.3. Closure condition

At the last step, $k = N - 1$, we need to get a closed loop $\vec{F}_N = \vec{F}_0$. This is one more constraint on the complex vectors $\vec{q}_0, \ldots \vec{q}_{N-1}$

$$\sum_0^{N-1} \vec{q}_k = 0; \tag{58}$$

We use this complex vector constraint to fix the arbitrary initial complex vector $\vec{F}_0$ as a function of all remaining parameters.

Due to the closure of the space loop $\vec{C}(\theta)$, the global translation of the momentum loop $\vec{P}(\theta)$ leaves invariant the Wilson loop; therefore, the translational zero modes of the momentum loop do not lead to ambiguities.

The circulation must correspond to a real number, though the Wilson loop is not real, as there is an asymmetry in the distribution of signs of circulation.

We discuss this issue in the following sections.

2.4. Mirror pairs of solutions

Return to the general study of the discrete loop equations (52).

There is a trivial solution to these equations at any even N

$$\vec{f}_k = \frac{(-1)^k \vec{q}}{2}; \tag{59}$$
$$\vec{q}^2 = 1; \tag{60}$$

We reject this solution as unphysical: the corresponding vorticity equals zero, as all the vectors $\vec{f}_k$ are aligned.

Our set of equations has certain mirror reflection symmetry

$$\vec{F}_k \leftrightarrow \vec{F}_{N-k}^* \tag{61}$$

Thus, the complex solutions come in mirror pairs $\vec{F}_k, \vec{F}_{N-k}^*$. The real solutions are only a particular case of the above trivial solution with real $\vec{q}$.

Each nontrivial solution represents a periodic random walk in complex vector space $\mathbb{C}^d$. The complex unit step $\vec{q}_k \in \mathbb{C}^d$ depends on the current position $\vec{F}_k \in \mathbb{C}^d$, or, equivalently, on the initial position $\vec{F}_0$ plus the sum of the preceding steps.

We are interested in the limit of infinitely many steps $N \to \infty$, corresponding to a closed fractal curve with a discontinuity at every point.

2.5. The degenerate fixed point and its statistical meaning

This solution's degeneracy (fewer restrictions than the number of free parameters) is a welcome feature. One would expect this from a fixed point of the Hopf equation for the probability distribution.

In the best-known example, the microcanonical Gibbs distribution covers the energy surface with a uniform measure (ergodic hypothesis, widely accepted in Physics).

The parameters describing a point on this energy surface are not specified– in the case of an ideal Maxwell gas, these are arbitrary velocities of particles.

Likewise, the fixed manifold, corresponding to our fractal curve, is parametrized by $N \to \infty$ sign variables, like an Ising model, plus an arbitrary global rotation matrix $\hat{O} \in SO(d)$, as discussed in the next Section.

This rich internal random structure of our fixed manifold, combined with its rotation and translation invariance in loop space C, makes it an acceptable candidate for extreme isotropic Turbulence.

3. Exact analytic solution

3.1. Random walk on a circle

How could a complex curve describe real circulation? This magic trick is possible if the imaginary part of $\vec{P}(\theta)$ does not depend on θ.

Such an imaginary term will drop after integration over closed loop $\vec{C}(\theta)$.

We have found a family of such solutions [32] of our recurrent equation (51) for arbitrary N

$$\vec{F}_k = \frac{1}{2} \csc\left(\frac{\beta}{2}\right) \left\{ \cos(\alpha_k), \sin(\alpha_k)\vec{w}, i\cos\left(\frac{\beta}{2}\right) \right\}; \tag{62}$$

Here $\vec{w} \in \mathbb{S}^{d-3}$ is a unit vector.

The angles α_k must satisfy recurrent relation

$$\alpha_{k+1} = \alpha_k + \sigma_k \beta; \tag{63}$$

$$\alpha_N = \alpha_0 = 0; \tag{64}$$

$$\sigma_k^2 = 1 \tag{65}$$

This sequence with arbitrary signs $\sigma_k = \pm 1$ solves recurrent equation (51) independently of γ.

The closure condition requires certain relations between these numbers.

The main condition is that β must be a rational fraction of 2π:

$$\beta = \frac{2\pi p}{q}; 0 < p < q < N \tag{66}$$

In that case, the periodic solution for α_k will have correspond to the following set of σ_k

$$\sigma = \{1, \ldots, 1, -1, \ldots, -1\}_{perm}; \tag{67}$$

This array has N_+ positive values and N_- negative values where

$$N_\pm = \left\lfloor \frac{N \pm q}{2} \right\rfloor; \tag{68}$$

$$N_+ + N_- = N; \tag{69}$$

$$N_+ - N_- = q - (N + q) \pmod 2; \tag{70}$$

The symbol *perm* stands for a random permutation of the array, which preserves its sum

$$\sum \sigma_k = (N_+ - N_-) \tag{71}$$

This sum must be a multiple of q for periodicity, which leads to another restriction

$$(N + q) \pmod 2 = 0 \tag{72}$$

In other words, q must have the same parity as N. These properties lead to periodicity

$$\alpha_N - \alpha_0 = \beta \sum \sigma_k = 2\pi p \tag{73}$$

Naturally, the sequence with all spins flipped: $\sigma_k \Rightarrow -\sigma_k$ also solves the loop equation. This sequence is a reflected solution we mentioned, so we include it in the statistical samples with equal probability.

The $\mathbb{Z}_2^{\otimes(N-1)}$ freedom of choosing $N - 1$ signs, σ_k, is a manifestation of a similar symmetry we observed before, with the random walk.

However, the random rational number $\frac{p}{q}$ we must use to describe our fixed point is new and unexpected. In the limit $N \to \infty$, this becomes a continuous random variable between zero and one. At finite N, we have to replace this random variable by its rational approximation with the denominator $q < N$ (same parity as N). After that, we can generate the sequence of angles $\sum \pm \beta$, adding up to a multiple of 2π.

The vectors $\vec{F}_k$ as solutions of the recurrent equation (51) are unique, however, the circulation and therefore all observables are invariant under shift of all $\vec{F}_k$ by a constant vector:

$$\vec{F}_k \Rightarrow \vec{F}_k + \vec{V} \tag{74}$$

This translation invariance follows from the closure of the loop C: any constant term in $\vec{F}(\theta)$ yields zero after integration $\oint d\vec{C} = 0$, or summation $\sum \Delta \vec{C} = 0$.

Using this translational invariance, we can drop the last component of $\vec{F}_k$ so that they become real vectors

$$\vec{F}_k \Rightarrow \frac{1}{2} \csc\left(\frac{\beta}{2}\right) \{\cos(\alpha_k), \sin(\alpha_k)\vec{w}, 0\}; \tag{75}$$

The vorticity operator will become a purely imaginary vector in the z direction:

$$\vec{\omega}_k = \left\{0, 0, \imath \frac{\sin(\beta \sigma_k)}{2(1 - \cos \beta)}\right\} \tag{76}$$

As we shall see, this does not lead to complex numbers for the correlation functions of vorticity in physical space.

The correlation function of two vorticities, separated by a finite distance $\vec{r}$ in an "inertial interval," is finite and real after integration over the global rotation matrix. Its limit at $\vec{r} \to 0$ may be singular so that the anomalous dissipation may emerge.

The random walk step $\vec{q}_k = \vec{F}_{k+1} - \vec{F}_k$ is a real unit vector in this solution

$$\vec{q}_k = \sigma_k\{-\sin\delta_k, \vec{w}\cos\delta_k, 0\}; \tag{77}$$

$$\delta_k = \alpha_k + \frac{\beta\sigma_k}{2} \tag{78}$$

The direction of this vector is not random, though; in addition to the random sign σ_k and random unit vector $\vec{w}$ in $d > 3$ dimensions, its direction depends on the previous position α_k on a circle.

So, this is a perfect example of a periodic Markov chain, with the periodicity condition analytically solved by quantizing the angular step to a rational number $\beta = \frac{2\pi p}{q}$.

This solution corresponds to the real value of velocity circulation on each of these two solutions; however, the reflection changes this value.

Thus, the arithmetic average of two Wilson loops with two reflected solutions is reflection-symmetric, but it is still a complex number.

This simple algorithm describes a valid solution of the loop equation for the statistical distribution of the Wilson loop in decaying Turbulence.

3.2. RandomFractions

Let us count all distinct fractions with denominator $q < N$ and proper parity, same as N. At given $q < N$ the allowed values of p are all integers $0 < p < q$ such that $\mathbf{gcd}(p, q) = 1$. Thus, (with $\delta[k]$ standing for Kronecker delta) it is related to the Euler totient function $\phi(n)$

$$CDF(x) = \lim_{N\to\infty} \frac{W_{Nx,N} + W_{Nx,N+1}}{2}; \tag{79}$$

$$CDF_{q,N} = \frac{\delta[(N-q) \ (\mathrm{mod}\ 2)]\phi(q)}{\sum_{q'=2}^{N-1} \delta[(N-q') \ (\mathrm{mod}\ 2)]\phi(q')} \tag{80}$$

$$\phi(n) = \sum_{p=1}^{n-1} \delta[\mathbf{gcd}(p, n) - 1] \tag{81}$$

The arithmetic mean of $W_{Nx,N}, W_{Nx,N+1}$ eliminates the restriction on the parity of q in the statistical limit $N \to \infty$. At given parity of N, half of the integers below N have a proper parity; another half of the integers would correspond to $N + 1$.

The tail of the probability distribution we are looking to, reduces to the following

$$W(x) = \frac{\delta[(N-q) \ (\mathrm{mod}\ 2)]\phi(q)}{\sum_{q'=2}^{N-1} \delta[(N-q') \ (\mathrm{mod}\ 2)]\phi(q')} \tag{82}$$

This prevented us from using the deterministic definition at $N \sim 10^{10}$, where the probabilistic one works fast enough for a personal workstation.

In conclusion, we observed the following distribution of our variables $q/N, p/q$ in the statistical limit

$$Prob[0 < p < q < N] = W\left(\frac{q}{N}, \frac{p}{q}\right) \tag{83}$$

$$W(x, y) \approx \left(1 - (1-x)^\mu \exp\left(\alpha + \beta x + \gamma x^2\right)\right) y; \tag{84}$$

There is no doubt that the number theory either already has or will soon produce the complete solution for this distribution, given its significance to the theory of turbulence.

3.3. Correlation functions and their numerical simulations

In this section, we only consider the three-dimensional space we live in. There are interesting mathematical problems related to decaying Turbulence in higher dimensions, which we leave to future researchers.

The simplest observable quantities we can extract from the loop functional are the vorticity correlation functions [18], corresponding to the loop C backtracking between two points in space $\vec{r}_1 = 0, \vec{r}_2 = \vec{r}$, see Fig.1. The vorticity operators are inserted at these two points.

The correlation function reduces to the following average over the ensemble of our random curves in complex space

$$
\left\langle \vec{\omega}(\vec{0}) \cdot \vec{\omega}(\vec{r}) \right\rangle = \frac{1}{4(t + t_0)^2}
$$

$$
\sum_{0 \leq n < m < N} \left\langle \vec{\omega}_m \cdot \vec{\omega}_n \exp\left(\frac{\imath \vec{r} \cdot \left(\vec{S}_{n,m} - \vec{S}_{m,n} \right)}{2\sqrt{\nu(t + t_0)}} \right) \right\rangle; \tag{85}
$$

$$
\vec{S}_{m,n} = \frac{\sum_m^n \vec{F}_k}{n - m \pmod{N}}; \tag{86}
$$

The averaging $\langle \dots \rangle$ in these formulas involves group integration $\int_{O(3)} d\hat{O}$ with $\vec{F}_k \Rightarrow \hat{O} \cdot \vec{F}_k$.

Let us explain the origin of summation over two positions n, m of the points $\vec{r}_1 = 0, \vec{r}_2 = \vec{r}$ on the discreet loop $\vec{C}(\theta)$.

Theoretically, in continuum limit $N \to \infty$, there is a degree of freedom we did not specify until now, namely, the reparametrization of the momentum loop $\vec{P}(\theta)$.

The loop equations (24) are invariant under the one-dimensional diffeomorphisms (or reparametrizations)

$$
\vec{P}(\theta) \Rightarrow \vec{P}(f(\theta)); \tag{87}
$$

$$
f'(\theta) > 0, f(2\pi) = f(0) + 2\pi \tag{88}
$$

Thus the general solution involves an arbitrary monotonous function $f(\theta)$, and averaging over the fixed manifold of the solutions of the Navier-Stokes equations involves functional integration over all such functions.

This integration includes summation over the positions θ_1, θ_2 of the vorticity insertion points on a curve $\vec{C}(\theta)$. In the continuum theory, this would be an ordered Lebesgue integration (diffeomorphisms preserve the ordering of points on a curve)

$$
\iint_{-\pi}^{\pi} \Theta(\theta_2 - \theta_1) \left(\vec{P}(\theta_1) \times d\vec{P}(\theta_1) \right) \otimes \left(\vec{P}(\theta_2) \times d\vec{P}(\theta_2) \right) \tag{89}
$$

and in our case of piecewise constant curve with discontinuities $\Delta \vec{P}_k$, it becomes an ordered sum

$$
\sum_{0 \leq n < m < N} \left(\vec{P}_m \times \Delta \vec{P}_m \right) \otimes \left(\vec{P}_n \times \Delta \vec{P}_n \right) \tag{90}
$$

The discontinuity $\Delta \vec{P}(\theta)$ stays finite in the continuum limit. The continuum limit can be taken only after integrating(summing) the internal degrees of freedom of the fixed manifold of the Loop equations.

The imaginary part of our solution (75) does not depend on the point on a circle. Therefore it contributes a constant term into $\vec{S}_{m,n}$ which cancels in the difference $\vec{S}_{n,m} - \vec{S}_{m,n}$ in the exponential, as it should.

The resulting integral over rotation matrix $\hat{O} \in O(3)$ is a particular case of the famous Itzykson-Zuber-Harish-Chandra integral[33]. There is a simple analytical formula

$$
\int_{O(3)} \frac{d\hat{O}}{|O(3)|} \exp(\imath \vec{r} \cdot \hat{O} \cdot \vec{s}) = \frac{\sin(|\vec{r}||\vec{s}|)}{|\vec{r}||\vec{s}|} \tag{91}
$$

Figure 1. Backtracking wires corresponding to vorticity correlation function.

The numerical simulation of this correlation function does not require significant computer resources. It is like a simulation of a one-dimensional Ising model with long-range forces. We simulated up to $N = 2 * 10^8$ with the random fraction in $\beta = 2\pi\frac{p}{q}$, $(q - N)$ mod $2 = 0$ and random signs σ_k adding up to a multiple of q. [34].

We took $T = 2 * 10^5$ random data samples for $\beta, \vec{\omega}_n \cdot \vec{\omega}_m, \left| \vec{S}_{n,m} - \vec{S}_{m,n} \right|$ with randomly chosen $0 \le n < m < N$. We collected the statistics $\sim 10^{13}$ data points needed for the correlation function. We ran it on an NYUAD cluster Jubail, which took about 14 hours on 200 nodes with 128 cores each.

The smaller simulation with $T = 10000$ took a couple of hours on the Linux workstation.

Computer resources on a cluster with n cores and m nodes grow as

$$RAM \approx 8 * N * n \text{ bytes per node}; \tag{92}$$
$$CPU \text{ time} \propto T / (n * m) \tag{93}$$

The distribution of β on Fig.2 is approximately linear and matches uniform random numbers. A Gauss-Kuzmin theorem describes a universal limit for the distribution of the deviation $\frac{p}{q} - f$ of our fraction from the uniform random number f used to approximate as a chain fraction [35].

The distribution of the difference $\Delta S = \left| \vec{S}_{n,m} - \vec{S}_{m,n} \right|$ on Fig.3 can be well fitted as a negative power

$$W(\Delta S > s) \approx A_{ds}s^{-\beta}; \tag{94}$$
$$\beta \approx 0.813; \tag{95}$$
$$A_{ds} \approx 3.568 * 10^{-4} \tag{96}$$

As for the correlation function (85) in the scaling region, it can be computed as follows.

The statistical distribution of these two variables $\Delta S, \vec{\omega}_m \cdot \vec{\omega}_n$ is a joint probability distribution.

We measured this dependence in a scattered log-log plot (Fig.4 by fitting log-log data to straight line for $N = (50M, 100M, 150M, 200M)$. Negative N stand for the negative correlations $-\vec{\omega}_m \cdot \vec{\omega}_n$. The results are consistent for these four values of N.
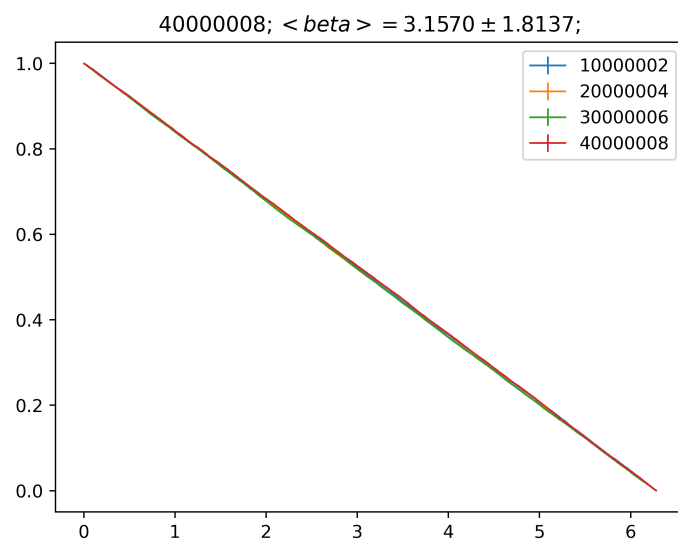
Figure 2. the distribution of the random fractional angle β in a log-log scale

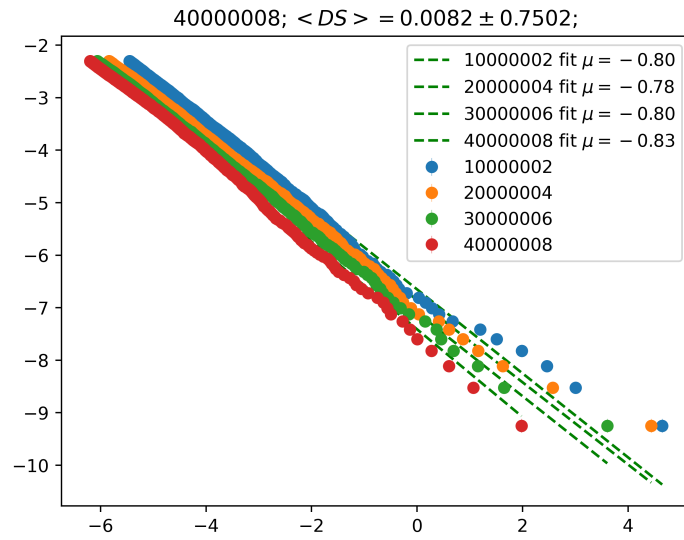**Figure 3.** The log-log plot of the CDF tail $W(\Delta S > s) \approx 3.568 * 10^{-4} s^{-\beta}$ of the length of the difference of average $\vec{F}$ vectors $\Delta S = \left|\vec{S}_{n,m} - \vec{S}_{m,n}\right|$, involved in vorticity circulation. This plot combines four sets with $N = (50M, 100M, 150M, 200M)$.
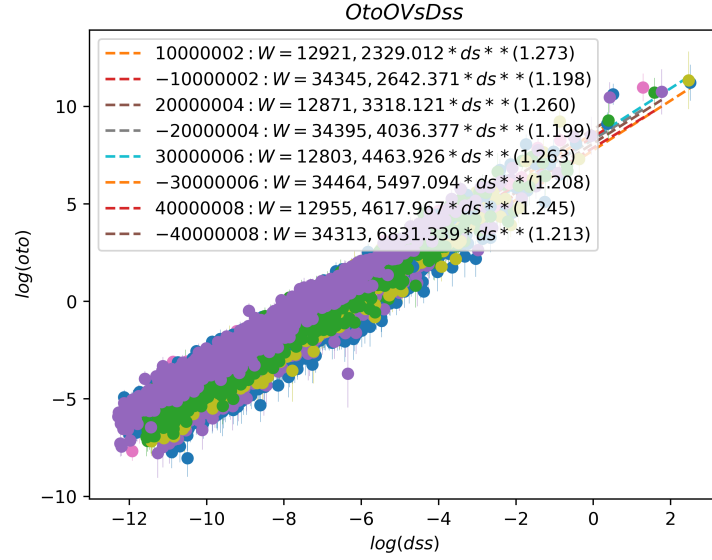
Figure 4. The cloud of points $\Delta S, \vec{\omega}_m \cdot \vec{\omega}_n$, in a log-log scale for various N. The linear fit corresponds to power laws for $N = (50M, 100M, 150M, 200M)$. Negative N stand for the negative correlations $-\vec{\omega}_m \cdot \vec{\omega}_n$. The results are consistent for these four values of N.
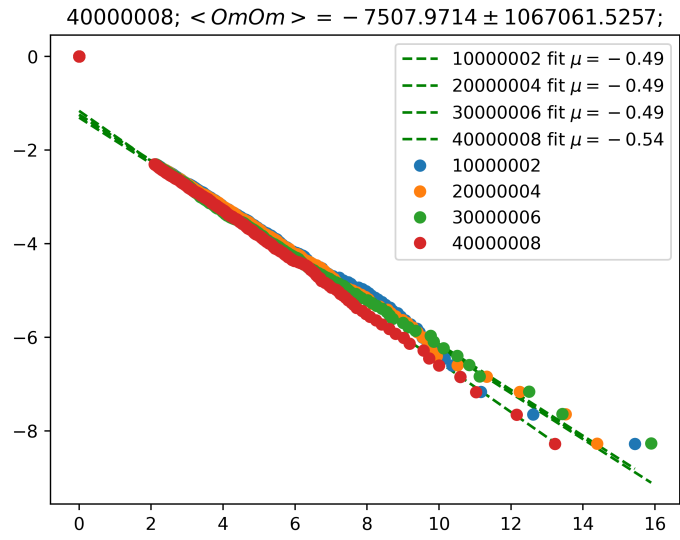
Figure 5. The log-log plot of the CDF tail $W(\vec{\omega}_m \cdot \vec{\omega}_n > w) \approx 2.828 * 10^{-1} w^{-0.503}$, involved in vorticity circulation. This plot combines four sets with $N = (50M, 100M, 150M, 200M)$. The fat tail $w^{-0.503}$ leads to a divergent expectation value.

There are two possibilities, with corresponding numbers of samples (we take the largest set, with $N = 200M$ points on a fractal curve)

$$\vec{\omega}_m \cdot \vec{\omega}_n \approx A_+ (\Delta S)^{\mu_+}; \; if \; \vec{\omega}_m \cdot \vec{\omega}_n > 0 \tag{97}$$

$$A_+ = 13851.157; \tag{98}$$

$$\mu_+ = 1.256; \tag{99}$$

$$S_+ = 128927 \; samples \tag{100}$$

and

$$\vec{\omega}_m \cdot \vec{\omega}_n \approx -A_- (\Delta S)^{\mu_-}; \; if \; \vec{\omega}_m \cdot \vec{\omega}_n < 0 \tag{101}$$

$$A_- = 15988.304; \tag{102}$$

$$\mu_- = 1.200; \tag{103}$$

$$S_- = 345312 \; samples \tag{104}$$

After that, the correlation can be computed analytically [36] using these scaling laws

$$\left\langle \vec{\omega}(\vec{0}) \cdot \vec{\omega}(\vec{r}) \right\rangle \approx \sum_{\pm} \frac{w_{\pm}}{t^2} \int_0^\infty ds \frac{\sin(\rho s)}{\rho s} s^{\mu_{\pm} - \beta - 1} =$$

$$- \sum_{\pm} \frac{w_{\pm}}{t^2} \rho^{\beta - \mu_{\pm}} \cos\left(\frac{1}{2} \pi (\beta - \mu_{\pm}) \right) \Gamma(-\beta + \mu_{\pm} - 1); \tag{105}$$

$$w_{\pm} = \pm \frac{\beta A_{ds} S_{\pm} A_{\pm}}{4(S_+ + S_-)}; \tag{106}$$

$$\rho = \frac{r}{\sqrt{2\nu t}}; \tag{107}$$

Substituting the numbers, we get

$$\left\langle \vec{\omega}(\vec{0}) \cdot \vec{\omega}(\vec{r}) \right\rangle \approx \frac{1}{t^2} \left(0.752351 \left(\frac{2\nu t}{r^2} \right)^{0.2215} - 2.59419 \left(\frac{2\nu t}{r^2} \right)^{0.1935} \right) \tag{108}$$

This function is negative at $|\vec{r}| > 2.514 * 10^{-10} \sqrt{2\nu t}$ but below this small value, it changes sign and tends to $+\infty$ because the $0.2215 > 0.1935$.

Our run's precision does not allow us to study such small values of ρ: the large-scale simulation on a supercomputer would be needed for that.

We can get two more orders of magnitude in statistical data with a large computer cluster, giving us one more digit in the indexes $\mu_{\pm}, \beta$. Our Python code is on GitHub [34], available for download. It runs on a personal computer and an HPC.

Qualitatively, we see the phenomena of anomalous dissipation as the coefficient in front of the power of ΔS on Fig.4 grows with N:

$$(5787, 8832, 12160, 113851) \; for \; N = (50M, 100M, 150M, 200M). \tag{109}$$

Another way to detect anomalous dissipation is to measure the fat tail of the distribution of $\vec{\omega}_m \cdot \vec{\omega}_n$ (see Fig. 5). The CDF tail decreases only as $w^{-1/2}$, leading to divergent expectation $\langle \vec{\omega}_m \cdot \vec{\omega}_n \rangle = \infty$ in the scaling limit.

The experimental data fitted in[37] suggest the decay of the dissipation rate $\mathcal{E} \sim t^{-1-n}$ with $n \approx 1.2$ in contrast with our $n \approx 1 - 0.2215 \approx 0.78$.

This discrepancy is puzzling. Any power law for the vorticity correlation must have the form (by dimensional counting)

$$\left\langle \vec{\omega}(\vec{0}) \cdot \vec{\omega}(\vec{r}) \right\rangle = \frac{const}{t^2} \left(\frac{\nu t}{r^2} \right)^{\lambda} \tag{110}$$

The index λ must be **positive**, otherwise there will be no growth at $\vec{r} \to 0$, and hence, no anomalous dissipation

$$\mathcal{E} = \left[\nu \left\langle \vec{\omega}(\vec{0}) \cdot \vec{\omega}(\vec{r}_0) \right\rangle \right]_{\vec{r}_0 \to 0, \nu \to 0} \propto (\vec{r}_0^2)^{-\lambda} \nu^{1+\lambda} t^{\lambda-2} \to const \; ; \tag{111}$$

$$\vec{r}_0^2 \propto \nu^{\frac{\lambda+1}{\lambda}} \to 0 \; at \; \lambda > 0 \tag{112}$$

Our $\lambda = 0.2215$ satisfies this inequality, but the fit of decaying turbulence data in [37] corresponds to negative $\lambda = 1 - n \sim -0.2$, which contradicts the anomalous dissipation requirement.

We cannot explain this contradiction: perhaps the data fit in [37] did not reach a true turbulent limit corresponding to our regime.

There is also a possibility that the true fixed point has a wider set of parameters. We explored this possibility and found ways to expand our solution, but we have not found any practical algorithms.

3.4. Analytic formula for the distribution of Enstrophy

Let us find analytic formulas for observables of this remarkable statistical distribution, which is isomorphic to the Ising model on a circle with a random imaginary rational coupling constant. The one-dimensional Ising models are usually solvable, and this one is no exception.

The simplest quantity is the enstrophy related to our random variables in the previous Section.

The simulations suggest the divergence of the enstrophy in the statistical limit $N \to \infty$, in agreement with the anomalous dissipation property of the turbulent flow.

Setting $\vec{r} = 0$ in (85) (which is possible at finite N) we find the following relation

$$\left\langle \vec{\omega}(\vec{0})^2 \right\rangle = \frac{1}{4(t+t_0)^2} \sum_{0 \leq n < m < N} \left\langle \vec{\omega}_m \cdot \vec{\omega}_n \right\rangle_{\frac{p}{q}, \sigma} ; \tag{113}$$

where $\langle \dots \rangle_{\frac{p}{q}, \sigma}$ denotes averaging over $\frac{p}{q}$ and the Ising variables σ subject to the global constraint $\sum \sigma_k = q$.

The averaging over $\frac{p}{q}$ is tricky: no analytic formula enumerates all positive fractions below 1 with denominator $q < N$ the same parity as N. We shall average over $\frac{p}{q}$ last and start with averaging over spins σ_k, which is rather straightforward.

First, we simplify the dot product involved

$$\vec{\omega}_m \cdot \vec{\omega}_n = -\frac{1}{4} \cot^2 \left(\frac{\beta}{2} \right) \sigma_m \sigma_n \tag{114}$$

Now, using the one-dimensional Fourier integral for the global constraint on σ, we get the unconstrained average:

$$\langle \vec{\omega}_m \cdot \vec{\omega}_n \rangle_\sigma = -\frac{1}{4} \cot^2 \left(\frac{\beta}{2} \right) \int_{-\pi}^{\pi} \frac{d\omega}{2\pi} e^{\imath \omega q} \left\langle \exp \left(-\imath \omega \sum_0^{N-1} \sigma_r \right) \sigma_m \sigma_n \right\rangle_\sigma \tag{115}$$

This unconstrained average factorizes as for $m \neq n$

$$\left\langle \exp \left(-\imath \omega \sum_0^{N-1} \sigma_r \right) \sigma_m \sigma_n \right\rangle_\sigma = -\cos^{N-2} \omega \sin^2 \omega \tag{116}$$

The resulting ω integral is calculable by expressing

$$\cos^{N-2}(\omega) = 2^{2-N}(e^{\iota\omega} + e^{-\iota\omega})^{N-2}; \tag{117}$$

$$\sin^2 \omega e^{\iota q\omega} = 2^{-2}\left(2e^{\iota q\omega} - e^{\iota(q+2)\omega} - e^{\iota(q-2)\omega}\right) \tag{118}$$

and integrating the binomial expansion of $(e^{\iota\omega} + e^{-\iota\omega})^{N-2}$ with other factor over the unit circle.

The unit circle integration $\oint d\omega e^{il\omega} = 2\pi\delta_l$ leaves just three terms in binomial expansion, which can be further simplified to the following [1]

$$\oint \frac{d\omega}{2\pi} \sin^2 \omega e^{\iota q\omega} \cos^{N-2}\omega = \frac{2^{-N}(N - q^2)}{N(N^2 - 1)B\left(\frac{N+q}{2} + 1, \frac{N-q}{2} + 1\right)} \tag{119}$$

Multiplying by the number $\frac{N(N-1)}{2}$ of terms in the sum in (113) and remaining factors we get the following result

$$\left\langle \vec{\omega}(\vec{0})^2 \right\rangle_\sigma = \frac{\mathcal{T}(N, p, q)}{(t + t_0)^2}; \tag{120}$$

$$\mathcal{T}(N, p, q) = \frac{2^{-N-4} \cot^2\left(\frac{\pi p}{q}\right)(N - q^2)\Gamma(N - 1)}{\Gamma\left(\frac{1}{2}(N - q + 2)\right)\Gamma\left(\frac{1}{2}(N + q + 2)\right)} \tag{121}$$

In the same way (see Appendix), the higher moments of enstrophy are related to calculable integrals:

$$\left\langle (\vec{\omega}(\vec{0})^2)^n \right\rangle_\sigma = \frac{\mathcal{T}(N, p, q, n)}{(t + t_0)^{2n}}; \tag{122}$$

$$\mathcal{T}(N, p, q, n) = \frac{N! \cot^{2n}\left(\frac{\pi p}{q}\right)}{(N - 2n)!} 2^{-2-2n} \oint \frac{d\omega}{2\pi} e^{\iota q\omega} \cos^{N-2n}\omega \sin^{2n}\omega =$$

$$\frac{\cot^{2n}\left(\frac{\pi p}{q}\right)}{2^{2n+N+2}}\binom{N - 2n}{\frac{N-q}{2} - 2n} {}_2F_1\left(-2n, -\frac{N}{2} - \frac{q}{2}; -2n + \frac{N}{2} - \frac{q}{2} + 1; -1\right) \tag{123}$$

---

[1] for some mysterious reason, *Mathematica*®13 failed to compute this integral

The moments of the distribution can be summed up into the generating function (
with an imaginary source $\vec{J}$, corresponding to the Fourier transform of PDF):

$$Z(J, N, p, q) = \left\langle \exp\left(\imath \vec{J} \cdot \hat{\Omega} \cdot \vec{\omega}(\vec{0})\right) \right\rangle_{\Omega\sigma} =$$

$$\left\langle \frac{\sin\left(|\vec{J}||\vec{\omega}(\vec{0})|\right)}{\left(|\vec{J}||\vec{\omega}(\vec{0})|\right)} \right\rangle_\sigma = \sum_{n=0}^{\infty} (-1)^n |\vec{J}|^{2n} / (2n+1)! \left\langle (\vec{\omega}(0))^{2n} \right\rangle$$

$$\oint \frac{d\omega}{8\pi} e^{\imath q\omega} \cos^N \omega \sum_{n=0}^{\infty} N! / (N-2n)!(2n+1)! \left(\frac{\imath |\vec{J}| \cot\left(\frac{\pi p}{q}\right) \tan\omega}{4(t+t_0)} \right)^{2n} =$$

$$\int_0^1 dz \oint \frac{d\omega}{8\pi} e^{\imath q\omega} \cos^N \omega \sum_{n=0}^{\infty} \binom{N}{2n} \left(\frac{\imath z |\vec{J}| \cot\left(\frac{\pi p}{q}\right) \tan\omega}{4(t+t_0)} \right)^{2n} =$$

$$\int_0^1 dz \oint \frac{d\omega}{8\pi} e^{\imath q\omega} \cos^N \omega \frac{(1+\imath zx)^N + (1-\imath zx)^N}{2} =$$

$$\oint \frac{d\omega}{16\pi} e^{\imath q\omega} \cos^N \omega \frac{(1+\imath x)^{N+1} - (1-\imath x)^{N+1}}{\imath (N+1)x}; \tag{124}$$

$$x = \frac{|\vec{J}| \cot\left(\frac{\pi p}{q}\right) \tan\omega}{4(t+t_0)} \tag{125}$$

The next task is to average this generating function over the ensemble of fractions $\frac{p}{q}$
with $q < N$.

We have to use a discrete definition (79), as the continuum limit leads to divergent
integrals

$$Z(J, N) = \frac{\delta[(N-q) \,(\text{mod } 2)] Z(J, N, q)}{\sum_{q'=2}^{N-1} \delta[(N-q') \,(\text{mod } 2)] \sum_{p'=1}^{q'-1} \delta[\mathbf{gcd}(p', q') - 1]}; \tag{126}$$

$$Z(J, N, q) = \sum_{p=1}^{q-1} \delta[\mathbf{gcd}(p, q) - 1] Z(J, N, p, q) =$$

$$\oint \frac{d\omega}{8\pi} e^{\imath q\omega} \cos^N \omega$$

$$\sum_{p=1}^{q-1} \delta[\mathbf{gcd}(p, q) - 1] \frac{\left(1 + \imath \xi \cot\left(\frac{\pi p}{q}\right)\right)^{N+1} - \left(1 - \imath \xi \cot\left(\frac{\pi p}{q}\right)\right)^{N+1}}{2\imath (N+1)\xi \cot\left(\frac{\pi p}{q}\right)}; \tag{127}$$

$$\xi = \frac{|\vec{J}| \tan\omega}{4(t+t_0)} \tag{128}$$

This expression is finite. The dangerous case $\frac{p}{q} = 1/2$ where $\cot\left(\frac{\pi p}{q}\right) = 0$ represents a
spurious singularity, where the ratio equals 1 in the last sum.

However, the boundary values $p \sim 1, q - p \sim 1$ produce large contributions

$$\propto (\imath \xi q / \pi)^N \tag{129}$$

unless we have finite values of

$$w = \omega N; \tag{130}$$

$$x = q / N; \tag{131}$$

$$y = p / q; \tag{132}$$

In that case, we get a finite expression

$$\int dW(x, y) \int_{-\infty}^{\infty} \frac{dw}{8\pi} \frac{\cos(xw) \sin zw}{zw}; \tag{133}$$

$$z = \frac{J \cot(\pi y)}{(t + t_0)}; \tag{134}$$

The last integral over w computes to the following (given $x > 0$)

$$\int_{-\infty}^{\infty} \frac{dw}{8\pi} \frac{\cos(xw) \sin zw}{zw} = \frac{\theta(|z| - x)}{16|z|} \tag{135}$$

$$\int dy \tan(\pi y) = -\frac{\log(\cos(\pi y))}{\pi} \tag{136}$$

Now, remarkably, all the regions of large $\cot(\pi y)$ are eliminated, and we get our final result

$$Z(J, \infty) = \int dW(x, y) \frac{\theta(|z| - x)}{16|z|} = \int_0^1 dW(x) \int_0^1 dy \frac{\theta(|z| - x)}{16|z|} =$$

$$\frac{(t + t_0)}{16J} \int_0^1 dW(x) \left(\frac{\log\left(1 + \frac{x^2(t+t_0)^2}{J^2}\right)}{2\pi} - 1 \right) \tag{137}$$

4. The Wilson Loop and the Circulation Moments

The Wilson loop in our theory can be computed as a functional of the loop by the following method. We limit ourselves to the three-dimensional case:

$$\Psi[\gamma, C] = \left\langle \exp\left(\frac{\imath \oint d\vec{C}(\theta) \cdot \vec{F}(\theta)}{\sqrt{2\nu(t + t_0)}} \right) \right\rangle_F \tag{138}$$

We rewrite this Lebesgue integral over the closed loop C:

$$\Psi[\gamma, C] = \left\langle \exp\left(-\frac{\imath \oint \vec{C}(\theta) \cdot d\vec{F}(\theta)}{\sqrt{2\nu(t + t_0)}} \right) \right\rangle_F \rightarrow$$

$$\left\langle \exp\left(-\frac{\imath \sum_{k=1}^{N} \vec{C}(2\pi k/N) \cdot \vec{q}_k}{\sqrt{2\nu(t + t_0)}} \right) \right\rangle_F \tag{139}$$

The group integration is now involved in the averaging of the ensemble of our random loops $\vec{F}_k$:

$$\int_{O(3)} \frac{d\Omega}{|O(3)|} \exp\left(-\frac{\imath \sum_{k=1}^{N} \vec{C}(2\pi k/N) \cdot \hat{O} \cdot \vec{q}_k}{\sqrt{2\nu(t + t_0)}} \right) =$$

$$\int_{O(3)} \frac{d\Omega}{|O(3)|} \exp\left(\imath \operatorname{tr} \hat{\Omega} \cdot \hat{X} \right); \tag{140}$$

$$\hat{X} = -\frac{\sum_{k=1}^{N} \vec{q}_k \otimes \vec{C}(2\pi k/N)}{\sqrt{2\nu(t + t_0)}} \tag{141}$$

The matrix $\hat{X}$ is not symmetric but real, as the vectors $\vec{q}_k = \vec{F}_{k+1} - \vec{F}_k$ are real. These are unit vectors on a plane, equivalent to complex numbers

$$Q_k = q_{k,x} + \imath q_{k,y} = \imath \sigma_k \exp\left(\imath \frac{\beta \sigma_k}{2} \right) \prod_{l=0}^{k-1} \exp(\imath \beta \sigma_l); \tag{142}$$

The points on a unit circle $\xi_k = \exp\left(\frac{2\pi\iota p}{q}\sigma_k\right)$ are related to the Ising variables $\sigma_k = \pm 1, \sum_l \sigma_l = q$.

The Markov property (dependence of ξ_k from the previous one, ξ_{k-1}) makes this random walk nontrivial and leads to critical behavior.

We observe that even at the large time $t \gg t_0$ when the asymptotic fractal curve is already in place, there is a region of loop sizes

$$|C| \sim \sqrt{\nu t} \tag{143}$$

where the Wilson loop is a nontrivial universal functional of the rescaled loop $\vec{C}_t = \vec{C}/\sqrt{\nu t}$. We compute these group integrals in Appendix A

$$\Psi[\gamma, C] = \left\langle \int_{\mathbb{S}_3} \frac{(dq)}{|\mathbb{S}_3|} \exp\left(\iota q \cdot \hat{R} \cdot q\right) \right\rangle_F ; \tag{144}$$

$$R_{\lambda\rho} = 1/2\left(T_{ij}^{\lambda\rho} + T_{ij}^{\rho\lambda}\right) X_{ij}; \tag{145}$$

$$T_{ij}^{\alpha\beta} = 1/2\mathrm{tr}\,\sigma_i\tau_\alpha\sigma_j\tau_\beta^\dagger; \tag{146}$$

$$\tau_\alpha = \{1, \iota\vec{\sigma}\}; \; \alpha = (0, 1, 2, 3) \tag{147}$$

This integral over $\mathbb{S}_3$ only depends on invariants: four real eigenvalues of our real symmetric $4 \otimes 4$ matrix $\hat{R}$. We found a Python library (see Appendix A) for fast (tens of milliseconds) computation of Fourier integrals on a sphere.

The Wilson loop is a complex function despite its reflection invariance. In other words, the dissipative effects are present in a big way in our solution.

We postpone the numerical investigation of the Wilson loop in our theory of decaying Turbulence till the next publication, where we plan to run large-scale simulations on a supercomputer.

The moments of the circulation can be analytically computed, though. We start with the definition:

$$\Gamma_p = \frac{\left\langle \left(\sum_{k=1}^N \vec{C}_\Omega(2\pi k/N) \cdot \vec{q}_k\right)^p \right\rangle_{F,\Omega}}{(2\nu(t + t_0))^{\frac{p}{2}}}; \tag{148}$$

$$\vec{C}_\Omega(\theta) = \hat{\Omega} \cdot \vec{C}(\theta) \tag{149}$$

The dot products can be written in complex components

$$\vec{C}_\Omega(2\pi k/N) \cdot \vec{q}_k = \mathcal{C}_k Q_k^* + \mathcal{C}_k^* Q_k; \tag{150}$$

$$\mathcal{C}_k = \frac{(C_\Omega)_x(2\pi k/N) + \iota(C_\Omega)_y(2\pi k/N)}{2} \tag{151}$$

The generic term of the multinomial expansion here reads:

$$p! \oint \frac{d\omega \exp(\iota q\omega)}{2\pi} \left\langle \exp\left(-\iota\omega \sum \sigma\right) \prod_{l=1}^r \frac{(\mathcal{C}_{k_l} Q_{k_l}^*)^{n_l} (\mathcal{C}_{k_l}^* Q_{k_l})^{m_l}}{n_l! m_l!} \right\rangle_\sigma \tag{152}$$

Using (142), this generic term reduces to a discrete Fourier integral

$$\oint \frac{d\omega \exp(\iota q\omega)}{2\pi} \left\langle \exp\left(-\iota\omega \sum_l \sigma_l\right) \prod (\iota\sigma_{k_l})^{m_l - n_l} \exp\left(\iota\pi\frac{p}{q}\left((m_l - n_l)\sigma_{k_l} + 2\sum_{s=n_l+1}^{m_l} \sigma_s\right)\right) \right\rangle_\sigma \tag{153}$$

Averaging over σ yields superposition of terms

$$\oint \frac{d\omega}{2\pi} \exp(\iota q\omega) \cos^{N_1} \omega \sin^{N_2} \omega \cos^{N_3}\left(\omega - N_4\pi\frac{p}{q}\right) \tag{154}$$

which are calculable by the same method we used in the previous section.

The complete algorithm is coded in *Mathematica®* [**?**].

Here are the formulas for the first few moments

$$\dots \tag{155}$$

5. Discussion

5.1. The Duality of Turbulence

We have presented an analytical solution of the Navier-Stokes loop equations for the Wilson loop in decaying Turbulence as a functional of the shape and size of the loop in arbitrary dimension $d > 2$.

The solution expresses the probability distribution and expected value for the Wilson loop at any given moment t in terms of an ensemble of fractal loops in complex momentum space. The loop is represented by a polygon with $N \to \infty$ sides.

This statistical system is isomorphic to a one-dimensional Ising ring with an imaginary random rational coupling constant $\imath\beta = \frac{\imath\pi p}{q}$.

Simulation of such a system is straightforward, and its $N \to \infty$ limit is achievable even on a desktop computer.

Some global observables, such as the enstrophy, are calculable for an arbitrary finite N, as a function of N, p, q, after which the problem reduces to a universal problem of the number theory: what is a discrete distribution of random fractions?

The equivalence of a strong coupling phase of the fluctuating vector field to quantum geometry is a well-known phenomenon in gauge theory (the ADS/CFT duality), ringing a bell to the modern theoretical physicist.

In our case, this is a simpler quantum geometry: a fractal curve in complex space.

An expert in the traditional approach to Turbulence may wonder why the Loop equation's solutions have any relation to the velocity field's statistics in a decaying turbulent flow.

Such questions were raised and answered in the last few decades in the gauge theories, including QCD[5,7–9] where the loop equations were derived first [3,4].

Extra complications in the gauge theory are the short-distance singularities related to the infinite number of fluctuating degrees of freedom in quantum field theory. The Wilson loop functionals in coordinate space are singular in the gauge field theory and cannot be multiplicatively renormalized.

Fortunately, there is no short-distance divergence in the Navier-Stokes equations nor the Navier-Stokes loop dynamics. The Euler equations represent the singular limit, which, as we argued, should be resolved using singular topological solitons regularized by the Burgers vortex.

In the present theory, we keep viscosity constant and do not encounter any short-distance singularities. The anomalous dissipation is achieved in our solution via a completely different mechanism.

The loop equation describes the gauge invariant sector of the gauge field theory. Therefore, the gauge degrees of freedom are lost in the loop functional. However, the gauge-invariant correlations of the field strength are recoverable from the solutions of the loop equation[3,4].

5.2. Stokes-type functionals and vorticity correlations

There is no gauge invariance regarding the velocity field in fluid dynamics (though there is such invariance in the Clebsch variables [18]). The longitudinal, i.e., a potential part of the velocity, has a physical meaning – it is responsible for pressure and energy pumping. This part is lost in the loop functional but is recoverable from the rotational part (the vorticity) using the Biot-Savart integral.

In the Fourier space, the correlation functions of the velocity field are algebraically related to those of vorticity $\vec{v}_k = \frac{i\vec{k} \times \vec{\omega}_k}{\vec{k}^2}$. Thus, the general solution for the Wilson loop functional $\Psi[\gamma, C]$ allows computing both vorticity and velocity correlation functions.

We demonstrated that in the last two sections by computing the correlation function of vorticity in coordinate space and the anomalous dissipation related to the singular limit of this correlation function at small distances.

We numerically computed the scaling indexes of our theory, simulating the ensemble of our Ising spin chain with the rational angular shift at the closed loop.

5.3. Relation of our solution to the weak Turbulence

The solution of the loop equation with finite area derivative, satisfying Bianchi constraint, belongs to the so-called Stokes-type functionals [3], the same as the Wilson loop for Gauge theory and fluid dynamics.

The Navier-Stokes Wilson loop is a case of the Abelian loop functional, with commuting components of the vector field $\vec{v}$.

As we discussed in detail in [3,4,18], any Stokes-type functional $\Psi[\gamma, C]$ satisfying boundary condition at shrunk loop $\Psi[0] = 1$, and solving the loop equation can be iterated in the nonlinear term in the Navier-Stokes equations (which iterations would apply at large viscosity).

The resulting expansion in inverse powers of viscosity (weak Turbulence) exactly coincides with the ordinary perturbation expansion of the Navier-Stokes equations for the velocity field, averaged over the distribution of initial data or boundary conditions at infinity.

We have demonstrated in [2,18] (and also here, in Section 1.3) how the velocity distribution for the random uniform vorticity in the fluid was reproduced by a singular momentum loop $\vec{P}(\theta)$.

The solution for $\vec{P}(\theta)$ in this special fixed point of the loop equation was random complex and had slowly decreasing Fourier coefficients, leading to a discontinuity $\text{sign}(\theta - \theta')$ in a pair correlation function (38). The corresponding Wilson loop was equal to the Stokes-type functional (30).

Our general Anzatz (14) satisfies the loop equation and boundary condition at $\Psi[C = 0] = 1$. It has a finite area derivative, which obeys the Bianchi constraint, making it a Stokes-type functional.

5.4. Conclusion

The exact solution for $\vec{P}(\theta)$ in decaying Turbulence which we have found in this paper, leads to the Stokes functional $\Psi[\gamma, C]$ satisfying the boundary value $\Psi[0] = 1$ at the shrunk loop.

Therefore, it represents a statistical distribution in a stochastic Navier-Stokes flow, corresponding to the degenerate fixed point of the Hopf equation for velocity circulation. It sums up all the Wylde diagrams in the limit of vanishing random forces plus nonperturbative effects, which are missed in the Wylde functional integral.

Whether this exact solution is realized in Nature remains to be seen.

Data Availability

We generated new data for the nonlinear complex random walk and the enstrophy distribution using the *Mathematica*® code [32,38–41] and Python code [34]. All this code is available for download.

References

1. Migdal, A.A. Random Surfaces and Turbulence. In Proceedings of the Proceedings of the International Workshop on Plasma Theory and Nonlinear and Turbulent Processes in Physics, Kiev, April 1987; Bar'yakhtar, V.G., Ed. World Scientific, 1988, p. 460.

2. Migdal, A. Loop Equation and Area Law in Turbulence. In *Quantum Field Theory and String Theory*; Baulieu, L.; Dotsenko, V.; Kazakov, V.; Windey, P., Eds.; Springer US, 1995; pp. 193–231. https://doi.org/10.1007/978-1-4615-1819-8.

3. Makeenko, Y.; Migdal, A. Exact equation for the loop average in multicolor QCD. *Physics Letters B* **1979**, *88*, 135–137. https://doi.org/https://doi.org/10.1016/0370-2693(79)90131-X.

4. Migdal, A. Loop equations and $\frac{1}{N}$ expansion. *Physics Reports* **1983**, *201*.

5. Migdal, A. Momentum loop dynamics and random surfaces in QCD. *Nuclear Physics B* **1986**, *265*, 594–614. https://doi.org/https://doi.org/10.1016/0550-3213(86)90331-7.

6. Migdal, A. Second quantization of the Wilson loop. *Nuclear Physics B - Proceedings Supplements* **1995**, *41*, 151–183. https://doi.org/https://doi.org/10.1016/0920-5632(95)00433-A.

7. Migdal, A.A. Hidden symmetries of large N QCD. *Prog. Theor. Phys. Suppl.* **1998**, *131*, 269–307, [hep-th/9610126]. https://doi.org/10.1143/PTPS.131.269.

8. Anderson, P.D.; Kruczenski, M. Loop equations and bootstrap methods in the lattice. *Nuclear Physics B* **2017**, *921*, 702–726. https://doi.org/https://doi.org/10.1016/j.nuclphysb.2017.06.009.

9. Kazakov, V.; Zheng, Z. Bootstrap for lattice Yang-Mills theory. *Phys. Rev. D* **2023**, *107*, L051501, [arXiv:hep-th/2203.11360]. https://doi.org/10.1103/PhysRevD.107.L051501.

10. Ashtekar, A. New variables for classical and quantum gravity. *Physical Review Letters* **1986**, *57*, 2244–2247. https://doi.org/10.1103/PhysRevLett.57.2244.

11. Rovelli, C.; Smolin, L. Knot Theory and Quantum Gravity. *Phys. Rev. Lett.* **1988**, *61*, 1155–1158. https://doi.org/10.1103/PhysRevLett.61.1155.

12. Iyer, K.P.; Sreenivasan, K.R.; Yeung, P.K. Circulation in High Reynolds Number Isotropic Turbulence is a Bifractal. *Phys. Rev. X* **2019**, *9*, 041006. https://doi.org/10.1103/PhysRevX.9.041006.

13. Iyer, K.P.; Bharadwaj, S.S.; Sreenivasan, K.R. The area rule for circulation in three-dimensional turbulence. *Proceedings of the National Academy of Sciences of the United States of America* **2021**, *118*, e2114679118. https://doi.org/10.1073/pnas.2114679118.

14. Apolinario, G.; Moriconi, L.; Pereira, R.; valadão, V. Vortex Gas Modeling of Turbulent Circulation Statistics. *PHYSICAL REVIEW E* **2020**, *102*, 041102. https://doi.org/10.1103/PhysRevE.102.041102.

15. Müller, N.P.; Polanco, J.I.; Krstulovic, G. Intermittency of Velocity Circulation in Quantum Turbulence. *Phys. Rev. X* **2021**, *11*, 011053. https://doi.org/10.1103/PhysRevX.11.011053.

16. Parisi, G.; Frisch, U. On the singularity structure of fully developed turbulence Turbulence and Predictability. In Proceedings of the Geophysical Fluid Dynamics: Proc. Intl School of Physics E. Fermi; M Ghil, R.B.; Parisi, G., Eds. Amsterdam: North-Holland, 1985, pp. 84–88.

17. Migdal, A. Topological Vortexes, Asymptotic Freedom, and Multifractals. *MDPI Fractals and Fractional, Special Issue* **2023**, [arXiv:physics.flu-dyn/2212.13356].

18. Migdal, A. Statistical Equilibrium of Circulating Fluids. *Physics Reports* **2023**, *1011C*, 1–117, [arXiv:physics.flu-dyn/2209.12312]. https://doi.org/10.48550/ARXIV.2209.12312.

19. Migdal, A. Universal Area Law in Turbulence, 2019, [arXiv:1903.08613].

20. Migdal, A. Scaling Index $\alpha = \frac{1}{2}$ In Turbulent Area Law, 2019, [arXiv:1904.00900v2].

21. Migdal, A. Exact Area Law for Planar Loops in Turbulence in Two and Three Dimensions, 2019, [arXiv:1904.05245v2].

22. Migdal, A. Analytic and Numerical Study of Navier-Stokes Loop Equation in Turbulence, 2019, [arXiv:1908.01422v1].

23. Migdal, A. Turbulence, String Theory and Ising Model, 2019, [arXiv:1912.00276v3].

24. Migdal, A. Towards Field Theory of Turbulence, 2020, [arXiv:hep-th/2005.01231].

25. Migdal, A. Probability Distribution of Velocity Circulation in Three Dimensional Turbulence, 2020, [arXiv:hep-th/2006.12008].

26. Migdal, A. Clebsch confinement and instantons in turbulence. *International Journal of Modern Physics A* **2020**, *35*, 2030018, [arXiv:hep-th/2007.12468v7]. https://doi.org/10.1142/s0217751x20300185.

27. Migdal, A. Asymmetric vortex sheet. *Physics of Fluids* **2021**, *33*, 035127. https://doi.org/10.1063/5.0044724.

28. Migdal, A. Vortex sheet turbulence as solvable string theory. *International Journal of Modern Physics A* **2021**, *36*, 2150062, [https://doi.org/10.1142/S0217751X21500627]. https://doi.org/10.1142/S0217751X21500627.
29. Migdal, A. Confined Vortex Surface and Irreversibility. 1. Properties of Exact solution, 2021, [arXiv:physics.flu-dyn/2103.02065v10].
30. Migdal, A. Confined Vortex Surface and Irreversibility. 2. Hyperbolic Sheets and Turbulent statistics, 2021, [arXiv:physics.flu-dyn/2105.12719].
31. Wikipedia. Burgers vortex. https://en.wikipedia.org/wiki/Burgers_vortex, 2022. [Online; accessed 27-April-2022].
32. Migdal, A. Symmetric Fixed Point. https://www.wolframcloud.com/obj/sasha.migdal/Published/SymmetricFixedPoint.nb, 2023.
33. McSwiggen, C. The Harish-Chandra integral: An introduction with examples, 2021, [arXiv:math-ph/1806.11155].
34. Migdal, A. LoopEquations. https://github.com/sashamigdal/LoopEquations.git, 2023.
35. Wikipedia contributors. Gauss–Kuzmin distribution — Wikipedia, The Free Encyclopedia, 2023. [Online; accessed 24-July-2023].
36. Migdal, A. Corr Function Integrals. https://www.wolframcloud.com/obj/sasha.migdal/Published/CorrFunctionIntegrals.nb, 2023.
37. Panickacheril John, J.; Donzis, D.A.; Sreenivasan, K.R. Laws of turbulence decay from direct numerical simulations. *Philosophical Transactions of the Royal Society A: Mathematical, Physical and Engineering Sciences* **2022**, *380*, 20210089, [https://royalsocietypublishing.org/doi/pdf/10.1098/rsta.2021.008 https://doi.org/10.1098/rsta.2021.0089.
38. Migdal, A. Complex Nonlinear Random Walk. https://www.wolframcloud.com/obj/sasha.migdal/Published/FQequation.nb, 2023.
39. Migdal, A. Moving Four Vertices. https://www.wolframcloud.com/obj/sasha.migdal/Published/MovingFourVertices.nb, 2023.
40. Migdal, A. Restricted O(3) Fourier Integral. https://www.wolframcloud.com/obj/sasha.migdal/Published/SphericalThetaIntegral.nb, 2023.
41. Migdal, A. Matrix Fourier Transform in S3. https://www.wolframcloud.com/obj/sasha.migdal/Published/ThetaIntegral.nb, 2023.
42. Schlömer, N. QuadPy. https://github.com/sigma-py/quadpy.git, 2023.

Appendix A The $O(3)$ group average

The correlation function (85) involves an integral over the $O(3)$ group

$$Q(\vec{r}, \vec{s}) = \int_{O(3)} \frac{d\Omega}{|O(3)|} \exp\left(\imath \vec{r} \cdot \hat{O} \cdot \vec{s}\right); \tag{A156}$$

with the vector $\vec{s}$ related to our fractal curve $\vec{F}(\theta)$ in a particular sample in our ensemble.

Both vectors $\vec{r}, \vec{s}$ are real.

This integral is a particular case of a Harish-Chandra-Itzykson-Zuber integral formula [33],

$$\int_{U(n)} e^{\mathrm{tr}(AUBU^*)} dU = \left(\prod_{p=1}^{n-1} p!\right) \frac{\det\left[e^{a_i b_j}\right]}{\Delta(A)\Delta(B)} \tag{A157}$$

where

$$\Delta(A) = \prod_{i<j}(a_j - a_i) \tag{A158}$$

is the Vandermonde determinant.

In our case, $O(3) = \left(\frac{SU(2)}{\mathbb{Z}_2}\right)$, so we use $n = 2$ formula with

$$A = \imath\sigma_i r_i, \ \Delta(A) = 2\imath|\vec{r}| \tag{A159}$$

$$B = \sigma_j s_j, \ \Delta(B) = 2|\vec{s}| \tag{A160}$$

$$\det\left[e^{a_i b_j}\right] = 2\imath \sin(|\vec{r}||\vec{s}|) \tag{A161}$$

where $\vec{\sigma}$ are Pauli matrices. With proper normalization to 1 at $\vec{r} = 0$, the HCIZ integral reads

$$\int_{O(3)} \frac{d\Omega}{|O(3)|} \exp\left(\imath \vec{r} \cdot \hat{O} \cdot \vec{s}\right) = \frac{\sin(|\vec{r}||\vec{s}|)}{|\vec{r}||\vec{s}|} \tag{A162}$$

Next, let us consider the case of the Fourier integral (140).
This integral does not reduce to the HCIZ integral and needs special treatment.
We use a quaternionic representation of $O(3)$ and write this integral:

$$Q(\hat{X}) = \int_{S_3} \frac{(dq)}{|S_3|} \exp\left(\imath q_\lambda q_\rho R_{\lambda\rho}\right); \tag{A163}$$

$$R_{\lambda\rho} = \frac{1}{2}\left(T_{ij}^{\lambda\rho} + T_{ij}^{\rho\lambda}\right) X_{ij}; \tag{A164}$$

$$T_{ij}^{\alpha\beta} = \frac{1}{2}\mathrm{tr}\,\sigma_i \tau_\alpha \sigma_j \tau_\beta^\dagger; \tag{A165}$$

$$\tau_\alpha = \{1, \imath\vec{\sigma}\};\ \alpha = (0, 1, 2, 3) \tag{A166}$$

In this representation, we have full $O(4)$ symmetry of this integral over unit sphere S_3 in four dimensions, plus there is a symmetry of the tensor $R_{\alpha\beta} = R_{\beta\alpha}$.

This Fourier integral can be computed in tens of milliseconds using a fast Python library **quadpy**[42]. It is optimized for integration over geometric shapes, including spheres in arbitrary dimensions. We licensed this library from the author and used it for our computations. Here is the code with its output for a random real symmetric tensor R

```python
def SphericalFourierIntegral(R):
    dim = 4
    scheme = quadpy.un.mysovskikh_2(dim)
    print("tol=", scheme.test_tolerance)
    vol = scheme.integrate(lambda x: np.ones(x.shape[1]), np.zeros(dim), 1.0)

    def func(x):
        return np.exp(1j * np.sum(x * (R.dot(x)), axis=0))/ vol
    return scheme.integrate(func, np.zeros(dim), 1.0)
    '''
    QuadPy.py::test_Fourie03Integral PASSED                          [100%]tol=
↪   1e-14

    quadpy: SphericalFourierIntegral = (-0.056352958761166728-0.012727710917488425j)
    quadpy O(3) Fourier Integral 28.73 ms

    '''
```